Predictable recovery rates in near-surface materials after earthquake damage
Non-peer reviewed preprint submitted to EarthArXiv.

Luc Illien[1,*], Jens M. Turowski[1], Christoph Sens-Schönfelder[1], Clément Berenfeld[3], and Niels Hovius[1,2]

[1]Helmholtz Center, GeoForschungsZentrum GFZ, Potsdam, 14473 , Germany
[2]Universität Potsdam, Department of Geosciences, Potsdam, 14476, Germany
[3]Universität Potsdam, Department of Mathematics, Potsdam, 14476, Germany
[*]Corresponding author, lillien@gfz-potsdam.de

ABSTRACT

Earthquakes introduce transient mechanical damage in the subsurface, which causes postseismic hazards and can take years to recover. This observation has been linked to relaxation, a phenomenon observed in a wide class of materials after straining perturbations, but its duration after earthquake ground shaking has not been constrained. Here, we analyse the effects of two successive large earthquakes and their aftershocks on ground properties using estimates of seismic velocity from ambient noise interferometry. We show that the relaxation time scale is a function of the state of the substrate at the time of seismic perturbation, rather than the intensity of ground shaking. Our study highlights the predictability of earthquake damage dynamics in the shallow subsurface and also in other materials. This finding may be reconciled with existing state variable frameworks by considering the superposition of different populations of damaged contacts.

Introduction

Earthquakes can cause catastrophic effects at the Earth's surface, which range from urban damage to physical changes in the landscape and hydrosphere[1,2]. For instance, landsliding[2], aquifer permeability[3] and river discharge[4] can peak after seismic strong ground motion, before eventually returning to pre-earthquake levels. Although they are transient, these effects can persist multiple years, increasing risk after major earthquakes[1].

Transient geomorphic and hydrologic phenomena are observed at the surface, but they suggest a change in the mechanical properties of the Earth's shallow subsurface in the aftermath of earthquakes. It has been found that earthquakes induce a drop in subsurface seismic velocity, which is followed by a recovery on time scales ranging from a few days to several years[5–7]. The recovery dynamics resemble universal relaxation[8], a phenomenon observed in rocks[9], granular media[10], concrete[11] and civil structures[12]. In the field, seismic velocity changes can be obtained through correlations of ambient seismic noise, a technique called seismic interferometry. The relaxation timescale observed with this method has been shown to correlate with the duration of enhanced postseismic landsliding in epicentral areas[13]. This suggests that the latter - and possibly other transient surface processes - originates from transient damage represented by the relaxation dynamics of the shallow subsurface. Hence, a physically based model with clear observables, to predict and constrain the duration of the recovery could strategically inform the hazard mitigation after earthquakes, and guide the monitoring of affected buildings, landscapes and fault zones.

The relaxation of earthquake-induced damage in subsurface materials is commonly analysed by fitting an exponential decay function to observed seismic velocity changes, with a single timescale[6,14]. This empirical method has yielded numerous relaxation timescales ranging from a few days to several years[7,13] but does not give insight into the main control of this duration. Moreover, the recovery of the seismic velocity changes exhibits a logarithmic evolution, which the exponential fit fails to capture[6]. It is clear that current practice provides an insufficient basis for reliable prediction of post-seismic recovery.

Motivated by this lack of physical framework and predictive power, models based on contact mechanics and friction physics have been recently used to explain observed velocity changes[15,16]. In these models, the rate of change of the velocity changes dv/dt is a direct function of the current state velocity $v(t)$. If these expressions are appropriate, then they permit the prediction of the relaxation duration from seismic velocity data. To date, seismic monitoring studies have mostly considered the impact of singular earthquakes, ignoring the potential importance of concatenated relaxations due to multiple seismic events. This hampers robust testing of models based on friction physics, and precludes their use in prediction and explanation of post-seismic relaxation.

Here, we aim to estimate daily seismic velocity changes in response to multiple earthquakes to improve current models of postseismic subsurface recovery in natural geological systems. The seismic station station PATCX in the Atacama desert of Chile (Fig. 1ab) was chosen for this study for three reasons. First, the site has experienced two major earthquakes, the 2007 Mw 7.7 Tocopilla and the 2014 Mw 8.2 Iquique, each with numerous aftershocks, giving the opportunity to study multiple episodes of cumulative damage and relaxation of the subsurface on relevant timescales. Second, previous work has demonstrated that the station records allow highly stable measurements of very small velocity changes[6, 17–19]. And third, the hyper-arid setting precludes significant effects of changes in water content ($\sim$ 1-5 mm/year of precipitation[20]). Using a 13-year time series of seismic velocity data for PATCX, we show that the timescales of recovery can be predicted from pre-earthquake seismic velocity values regardless of the initial ground shaking intensity.

13 years of seismic velocity changes induced by earthquake damage

The relative seismic velocity changes at the PATCX site are controlled by all forcings that modify rock properties in the subsurface. Notably, thermal strain at depth due to the seasonal temperature variations in the Atacama desert possibly masks the influence of earthquake damage[17]. We modelled these thermal effects with a simple 1D heat diffusion approach (Materials and Methods) to obtain residual relative velocity changes. In the absence of significant hydrological influences, we assume that these residual changes represent the response to seismic ground shaking (Fig. 1a). Then, we scaled the relative seismic velocity measurement to the reference value for the local shear velocity $V_S = 1500$ m/s[19]. The resulting time-series shows velocity drops of 15 and 35 m/s for the Tocopilla and Iquique earthquake, respectively. Each was followed by a recovery period of three to four years, the longer after the Iquique earthquake. Additional drops and associated recoveries due to aftershocks and smaller earthquakes are evident, particularly in the aftermath of the Tocopilla earthquake. Drop amplitudes have been shown to be proportional to the peak ground velocity at PATCX and other sites[6, 17].

We emphasize the log-linear behaviour of the post-seismic velocity recovery by plotting the first 1000 days of the recovery phases following the two large earthquakes on a logarithmic scale (Fig. 1c). For three orders of time magnitude, the recoveries after both large earthquakes appear linear in this space, with some deviations due to aftershocks. The consistency of the slope despite these additional perturbations suggests that the recovery timescale may be predictable by measuring the rate of velocity change in the first weeks after an earthquake, provided that other effects (e.g., hydrology) can be excluded.

We normalised the recoveries by considering the percentage of recovered change relative to the amplitude of the velocity drop (Fig. 1d). This normalisation collapses the time series for the two earthquakes onto a single line. This indicates that, although despite causing different drop magnitudes, both earthquakes induced a relaxation behaviour that had a similar timescale of recovery over the first 1000 post-seismic days. The co-seismic velocity reductions were approximately halved in the first 200 days of recovery following the main shocks. Aftershocks with smaller attendant velocity drops did not have a significant impact on the total relaxation duration. We estimate that, on average, the full recovery of the seismic velocity after Tocopilla and Iquique earthquakes would take about 10 years (Materials and Methods, Fig. S4a).

Pre-drop velocity level controls the timescale of recovery

We observed that the velocity immediately prior to ground shaking, as well as the recovery timescales were very similar after the Tocopilla and Iquique earthquakes. This suggests that the subsurface relaxation is a function of the medium properties rather than the initial intensity of that ground shaking. This hypothesis can be explored further by analysing the recoveries following aftershocks, extending the range of pre-drop velocity conditions prior to earthquakes. The first 10 days of recovery after each seismic event can be visualised and normalised by the pre-drop velocity level, here represented by the velocity on the day prior to the aftershock (Fig. 2a). A 10-day window was chosen to minimise the potential superposition of recoveries associated with previous aftershocks. In this time, recovery to the pre-aftershock baseline ranged from 20-30% for some aftershocks to 100% for others.

A correlation appears to exist between the seismic velocities just before aftershocks and the subsequent rate of recovery, with faster recovery for drops with lower pre-drop velocity (Fig. 2a). We quantified this trend by fitting the 10-day recovery histories with a universal relaxation function[23] (Materials and Methods, Fig. S4b). This yields a likely maximum relaxation timescales τ_{max} for each aftershock, where the value of τ_{max} represents the recovery time to the seismic velocity observed before the drop. The distribution of the inferred timescales τ_{max} for the aftershocks in our time series ranges from $\sim$ 8 to $\sim$ 3000 days and can be described by an exponential relationship ($R^2 = 0.86$) with the pre-drop velocity. This scaling suggests that at low velocities relative to a baseline in which the velocities seem to be at steady state (here $\sim$ 1500 m/s), the subsurface at PATCX may be more resilient with systematically shorter recovery times.

Using this fitted exponential relationship, we built a synthetic seismic velocity time-series. We measured all the velocity drops in the data, calculated their recovery timescale with their pre-drop velocity, and superposed them linearly, creating one time-series with multiple relaxations. Even if this synthetic time-series does not directly fit the full measured dataset, there is a
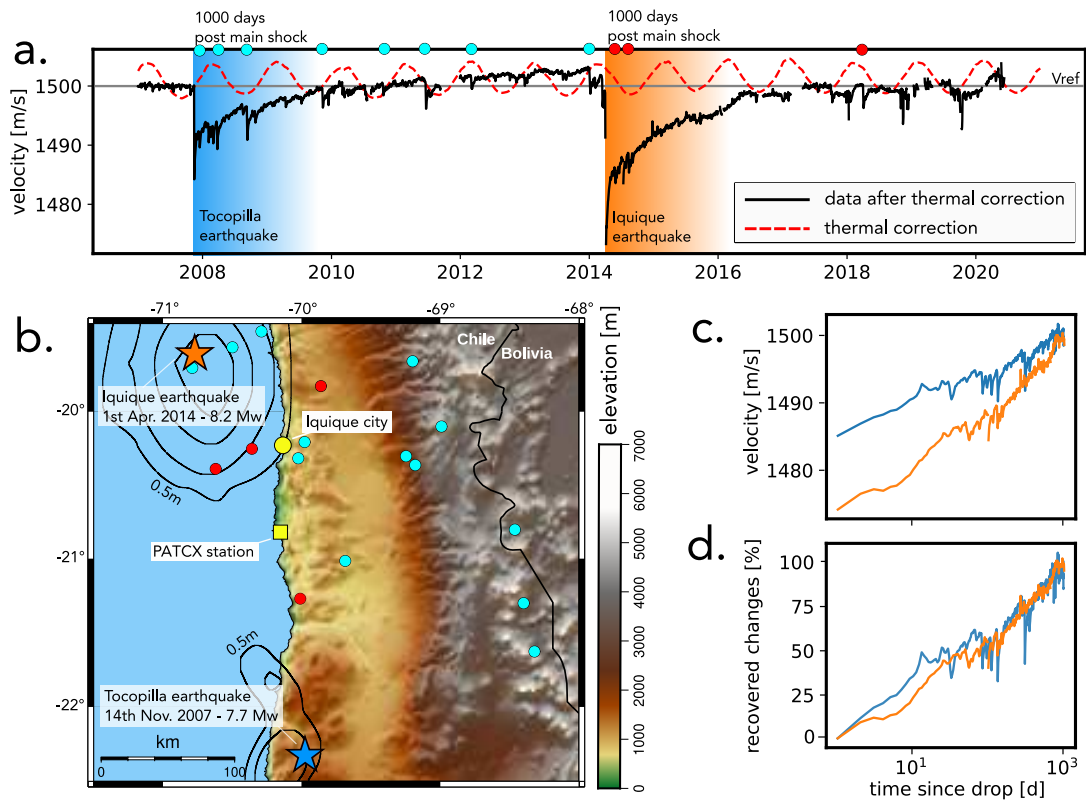
Figure 1. *13 years of seismic velocity data for Station PATCX in Chile, including transient changes due to the Tocopilla and Iquique earthquakes* **a.** The black-line indicates the relative seismic velocity changes plotted against a reference velocity of 1500 m/s (horizontal grey line). The red line shows the correction for thermal strain due to recorded temperature fluctuations. Dots at the top mark the occurence of aftershocks. **b.** Map showing the study area with stars indicating the epicenters of the main shocks[21,22] (0.5–1 m for the Tocopilla event and 0.5–3 m for the Iquique event). Red and cyan dots indicate the aftershocks inducing velocity drops (full list in Table S1) **c.** Plot of seismic velocity recovery during the first 1000 days following the main shocks on a logarithmic time-axis. The blue and orange lines are for the Tocopilla and the Iquique earthquake episode respectively. **d.** Plot of seismic velocity recoveries normalised by the amplitude of the respective initial velocity drop.

good overall agreement with the instrumental data (Fig. 2c, Nash-Sutcliff efficiency NSE =0.68, Materials and Methods), in contrast to a synthetic velocity time series calculated with a constant recovery time scale, as previously used[24] (red line in Fig. 2c, NSE = −2.61). The remaining offsets between the data and the synthetic time-series (particularly visible in the 2012-2014 period) may be due to the limitation of the temperature correction, a new persistent velocity base level following the Tocopilla earthquake or a draw-down of groundwater levels in the Atacama region[25], which could affect the velocity changes[26,27].

Which physical framework can describe near-surface earthquake damage ?

Our observations suggest that the timescale of seismic velocity recovery at a site can be predicted from the known pre-drop velocity. This feature is not directly tied to existing physical equations for relaxation. Most existing physical and conceptual models associate the relaxation dynamics to a 'state variable' representing the dynamics of the dominant type of contact or void embedded in a medium undergoing deformation. In these frameworks, the evolution of the variable of of interest, here dv/dt, is a direct function of the variable itself ($v(t)$). This is the case in the rate and state friction framework[28] and models that involve contact dynamics[29] and creeping mechanisms to fit relaxation data[15,16]. Field studies often test such models based on one relaxation event. Our dataset, comprising 18 consecutive drop-and-recovery cycles does not support this state variable approach. Importantly, the phase portrait of the relationship between the rate of velocity change dv/dt and the velocity $v(t)$ shows very different phase locations after each seismic event (Fig. S5) i.e., the same state velocity $v(t)$ can have different rates of variation dv/dt. Still, we suggest that a state variable argument can be reconciled with our observations.

In the field, seismic velocity measurements probe a subsurface volume that contains many types of contacts and flaws[9,23,30].
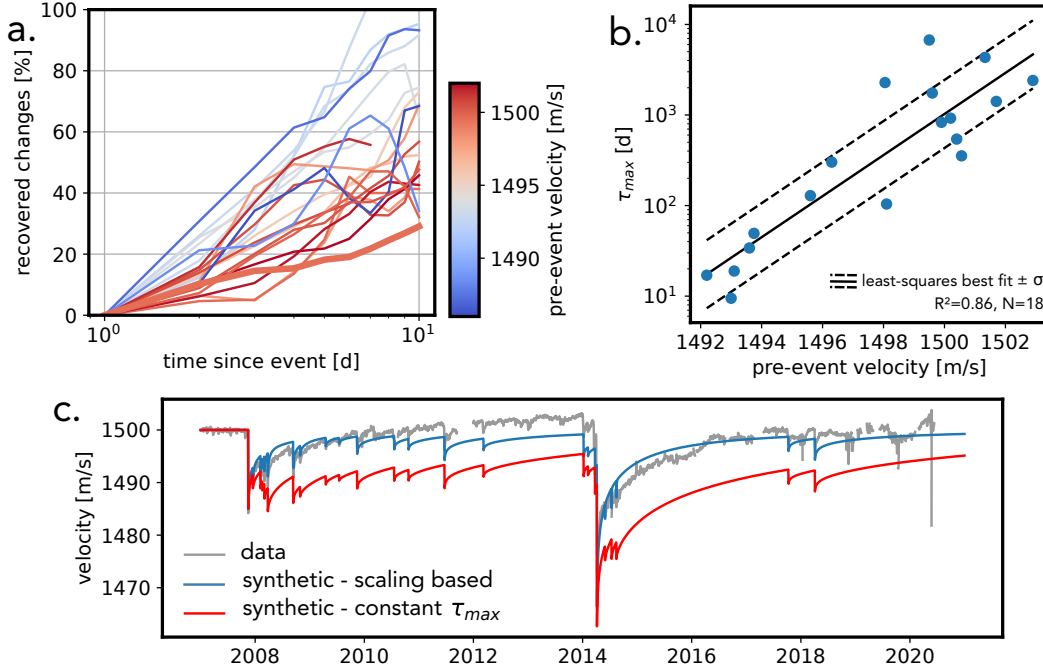
Figure 2. *Pre-drop velocity level as a control on the relaxation timescale and corresponding synthetic time-series.* **a.** Recoveries after individual seismic events, normalised by the amplitude of the drop. The colour indicates the relevant pre-drop velocity. The thick line shows the early average recovery observed after the Tocopilla and Iquique main shocks. **b.** Fitted maximum recovery timescales for the recoveries shown in **a** (N=18). The black lines show the best fit exponential scaling ($\tau_{max} = \exp(a*V_0 + b)$ for a = 5.22256*10^{-1} and b = - 7.764515*10^2) and its standard deviation. **c.** Synthetic velocity time-series built by superposition of relaxations obtained with the relationship shown in **b** (blue line) and for a constant relaxation timescale (in red and taken as 3887 d, the value fitted for the Iquique and Tocopilla recoveries). The grey line shows the instrumental data.

To account for their different dynamics, we assumed that all of these structures obey their own state variable equations, each with their timescale of relaxation. For instance, crack populations can be defined by their aspect ratios, which determine their time of closure under a specific load[31,32]. We used a generic state variable (Materials and Methods) that can characterise different processes, each with their own timescale (Fig. 3a). The simple mean of all these state variable dynamics yields a synthetic time-series with the same features as our seismic velocity observations: A logarithmic recovery of velocity after each drop at a rate dependent on the pre-drop velocity (Fig. 3bc). Therefore, the superposition of different timescales in a sequence of perturbations can reproduce the dynamics we observed at station PATCX (Fig. 3). This combined contribution of different states of evolution is key to reconciling observations and physics. At the reference velocity value (in our study around 1500 m/s), all contacts are at steady state and the system does not evolve. When the contacts are disturbed, they all enter a metastable state and recover at different rates. As the general reference velocity is approached, only the contact populations with the longest recovery times remain activated, while populations with a faster recovery have stabilized (Fig. 3). Assuming that the internal structures in the subsurface at a site are not fundamentally changed (no new types of contacts or flaws), we expect that the recovery of seismic velocity due to earthquakes can be predicted based on this theory.

Building upon the observation of universal relaxation in the lab[8], our study shows that after an earthquake, the mechanical properties of a subsurface medium control its relaxation behaviour and timescale of recovery, while the ground shaking intensity only controls the amplitude of the velocity change or the magnitude of damage. If this recovery behaviour is valid for near-surface geomaterials, then it may also be tested for man-made structures. Understanding the link between specific types of flaws and relaxation timescales can lead to a targeted material test for management of the response to damage. A representative relaxation timescale may also allow an estimation of the propensity to failure of steep topographic slopes in an earthquake epicentral area[13] and therefore an assessment of the feasibility and timeliness of reconstruction after large earthquakes. This can reduce lingering post-seismic risk, and minimize spurious investment. Finally, we propose that measuring the rate of velocity change over a period immediately after an episode of strong ground motion, can yield early constraints on the likely pace of recovery of substrate damage. This early estimation can be based on measurements from small seismic events to construct a

site-dependent relationship between pre-drop seismic velocity and the expected relaxation timescale as shown in Fig. 2b, and then upscaled for larger earthquakes.
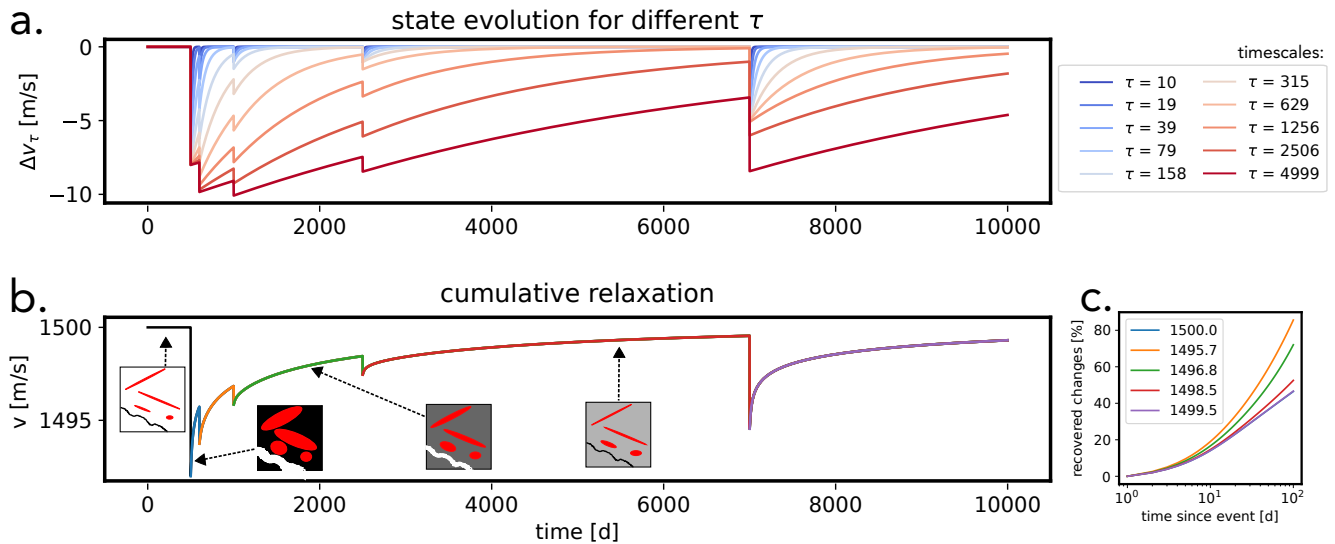
Figure 3. *Superposition of different state variable dynamics and average relaxation* **a.** Each curve shows the evolution of a hypothetical state variable with a distinct characteristic timescale. The timescales are shown in the legend. **b.** Average evolution of all state variables shown in **a**. The colours on the line stand for the recoveries after each drop (also shown in **c**). The schematics indicate different types of cracks/voids with different closure times corresponding to different state variables in **a**. The background colour indicates the relaxation of the stress state in the bulk. **c.** The first 100 days of the relaxation phases shown in **b.** are plotted on a log-linear scale and normalised by the amplitude of the initial drop. The colours indicate the value of the velocity before the drop onset on both plots **b.** and **c.**

References

1. Fan, X. *et al.* Earthquake-Induced Chains of Geologic Hazards: Patterns, Mechanisms, and Impacts, DOI: 10.1029/2018RG000626 (2019).

2. Marc, O., Hovius, N., Meunier, P., Uchida, T. & Hayashi, S. Transient changes of landslide rates after earthquakes. *Geology* **43**, 883–886, DOI: 10.1130/G36961.1 (2015).

3. Manga, M. *et al.* Changes in permeability caused by transient stresses: Field observations, experiments, and mechanisms. *Rev. Geophys.* **50**, DOI: 10.1029/2011RG000382 (2012).

4. Wang, C. Y., Wang, C. H. & Manga, M. Coseismic release of water from mountains: Evidence from the 1999 (Mw = 7.5) Chi-Chi, Taiwan, earthquake. *Geology* **32**, 769–772, DOI: 10.1130/G20753.1 (2004).

5. Brenguier, F. *et al.* Postseismic relaxation along the San Andreas fault at Parkfield from continuous seismological observations. *Sci. (New York, N.Y.)* **321**, 1478–81, DOI: 10.1126/science.1160943 (2008).

6. Gassenmeier, M. *et al.* Field observations of seismic velocity changes caused by shaking-induced damage and healing due to mesoscopic nonlinearity. *Geophys. J. Int.* **204**, 1490–1502, DOI: 10.1093/gji/ggv529 (2016).

7. Viens, L., Denolle, M. A., Hirata, N. & Nakagawa, S. Complex Near-Surface Rheology Inferred From the Response of Greater Tokyo to Strong Ground Motions. *J. Geophys. Res. Solid Earth* **123**, 5710–5729, DOI: 10.1029/2018JB015697 (2018).

8. TenCate, J. A., Smith, E. & Guyer, R. A. Universal slow dynamics in granular solids. *Phys. Rev. Lett.* **85**, 1020–1023, DOI: 10.1103/PhysRevLett.85.1020 (2000).

9. Shokouhi, P., Rivière, J., Guyer, R. A. & Johnson, P. A. Slow dynamics of consolidated granular systems: Multi-scale relaxation. *Appl. Phys. Lett.* **111**, DOI: 10.1063/1.5010043 (2017).

10. Knight, J. B., Fandrich, C. G., Ning Lau, C., Jaeger, H. M. & Nagel, S. R. Density relaxation in a vibration.pdf. *Phys. Rev. E* **51** (1995).

11. Bentahar, M. *et al.* Exploiting Slow Dynamics Effects for Damage Detection in Concrete. *Front. Built Environ.* **6**, 1–10, DOI: 10.3389/fbuil.2020.00064 (2020).

12. Astorga, A., Guéguen, P. & Kashima, T. Nonlinear elasticity observed in buildings during a long sequence of earthquakes. *Bull. Seismol. Soc. Am.* **108**, 1185–1198, DOI: 10.1785/0120170289 (2018).

13. Marc, O. *et al.* Toward Using Seismic Interferometry to Quantify Landscape Mechanical Variations after Earthquakes. *Bull. Seismol. Soc. Am.* 1–19, DOI: 10.1785/0120200264 (2021).

14. Hobiger, M., Wegler, U., Shiomi, K. & Nakahara, H. Single-station cross-correlation analysis of ambient seismic noise: application to stations in the surroundings of the 2008 Iwate-Miyagi Nairiku earthquake. *Geophys. J. Int.* **198**, 90–109, DOI: 10.1093/gji/ggu115 (2014).

15. Ostrovsky, L. *et al.* Long-Time Relaxation Induced by Dynamic Forcing in Geomaterials. *J. Geophys. Res. Solid Earth* **124**, 5003–5013, DOI: 10.1029/2018JB017076 (2019).

16. Wang, S. Y. *et al.* Near-surface softening and healing in eastern Honshu associated with the 2011 magnitude-9 Tohoku-Oki Earthquake. *Nat. Commun.* **12**, 1–10, DOI: 10.1038/s41467-021-21418-7 (2021).

17. Richter, T., Sens-Schönfelder, C., Kind, R. & Asch, G. Comprehensive observation and modeling of earthquake and temperature-related seismic velocity changes in northern Chile with passive image interferometry. *J. Geophys. Res. Solid Earth* **119**, 4747–4765, DOI: 10.1002/2013JB010695 (2014).

18. Sens-Schönfelder, C. & Eulenfeld, T. Probing the in situ Elastic Nonlinearity of Rocks with Earth Tides and Seismic Noise. *Phys. Rev. Lett.* **122**, DOI: 10.1103/PhysRevLett.122.138501 (2019).

19. Illien, L., Sens-Schönfelder, C. & Ke, K.-Y. Resolving minute temporal seismic velocity changes induced by earthquake damage: the more stations, the merrier? *Geophys. J. Int.* **234**, 124–135, DOI: 10.1093/gji/ggad038 (2023). https://academic.oup.com/gji/article-pdf/234/1/124/49401687/ggad038_supplemental_file.pdf.

20. Houston, J. Variability of precipitation in the Atacama Desert: Its causes and hydrological impact. *Int. J. Climatol.* **26**, 2181–2198, DOI: 10.1002/joc.1359 (2006).

21. Schurr, B. *et al.* The 2007 M7.7 Tocopilla northern Chile earthquake sequence: Implications for along-strike and downdip rupture segmentation and megathrust frictional behavior. *J. Geophys. Res. Solid Earth* **117**, DOI: https://doi.org/10.1029/2011JB009030 (2012).

22. Schurr, B. *et al.* Gradual unlocking of plate boundary controlled initiation of the 2014 Iquique earthquake. *Nature* **512**, 299–302, DOI: 10.1038/nature13681 (2014).

23. Snieder, R., Sens-Schönfelder, C. & Wu, R. The time dependence of rock healing as a universal relaxation process, a tutorial. *Geophys. J. Int.* **208**, 1–9, DOI: 10.1093/gji/ggw377 (2016).

24. Illien, L. *et al.* Seismic Velocity Recovery in the Subsurface: Transient Damage and Groundwater Drainage Following the 2015 Gorkha Earthquake, Nepal. *J. Geophys. Res. Solid Earth* **127**, 1–18, DOI: 10.1029/2021jb023402 (2022).

25. Viguier, B. *et al.* Water table variations in the hyperarid Atacama Desert: Role of the increasing groundwater extraction in the pampa del tamarugal (Northern Chile). *J. Arid Environ.* **168**, 9–16, DOI: https://doi.org/10.1016/j.jaridenv.2019.05.007 (2019).

26. Clements, T. & Denolle, M. A. Tracking Groundwater Levels Using the Ambient Seismic Field. *Geophys. Res. Lett.* **45**, 6459–6465, DOI: 10.1029/2018GL077706 (2018).

27. Illien, L. *et al.* Subsurface Moisture Regulates Himalayan Groundwater Storage and Discharge. *AGU Adv.* **2**, DOI: 10.1029/2021av000398 (2021).

28. Dieterich, J. H. Modeling of rock friction: 1. Experimental results and constitutive equations. *J. Geophys. Res. Solid Earth* **84**, 2161–2168, DOI: https://doi.org/10.1029/JB084iB05p02161 (1979).

29. Aharonov, E. & Scholz, C. H. A Physics-Based Rock Friction Constitutive Law: Steady State Friction. *J. Geophys. Res. Solid Earth* **123**, 1591–1614, DOI: 10.1002/2016JB013829 (2018).

30. Sens-Schönfelder, C., Snieder, R. & Li, X. A model for nonlinear elasticity in rocks based on friction of internal interfaces and contact aging. *Geophys. J. Int.* **216**, 319–331, DOI: 10.1093/gji/ggy414 (2019).

31. Budiansky, B., Hutchinson, J. W. & Slutsky, S. Void Growth and Collapse in Viscous Solids. In HOPKINS, H. G. & SEWELL, M. J. (eds.) *Mechanics of Solids*, 13–45, DOI: https://doi.org/10.1016/B978-0-08-025443-2.50009-4 (Pergamon, Oxford, 1982).

32. Meyer, G. G., Brantut, N., Mitchell, T. M., Meredith, P. G. & Plümper, O. Time Dependent Mechanical Crack Closure as a Potential Rapid Source of Post-Seismic Wave Speed Recovery: Insights From Experiments in Carrara Marble. *J. Geophys. Res. Solid Earth* **126**, 1–29, DOI: 10.1029/2020JB021301 (2021).

33. Sens-Schönfelder, C. & Wegler, U. Passive image interferemetry and seasonal variations of seismic velocities at Merapi Volcano, Indonesia. *Geophys. Res. Lett.* **33**, DOI: 10.1029/2006GL027797 (2006).

34. Schafer, R. W. What Is a Savitzky-Golay Filter? [Lecture Notes]. 111–117 (2011).

35. Turcotte, D. & Schubert, G. *Geodynamics* (Cambridge University Press, 2014), 3 edn.

36. Chartrand, R. Numerical differentiation of noisy, nonsmooth, multidimensional data. In *2017 IEEE Global Conference on Signal and Information Processing (GlobalSIP)*, 244–248, DOI: 10.1109/GlobalSIP.2017.8308641 (2017).

Supplementary materials

Materials and Methods

Seismic Interferometry: We computed the 6 self-correlations (EE, NN; ZZ, EN, EZ, NZ) of the PATCX station after filtering the traces in the 3-6 Hz band. Daily cross-correlations are extracted with a pre-processing scheme fully described in Illien et al., 2023). To measure the velocity changes, the stretching technique[33] was applied in the 7 to 16 seconds window of the daily correlation functions. The full method for averaging the 6 self-correlations is detailed in Illien et al., 2023.

Temperature-correction: We first quantified the phase of the periodic temperature (taken at the Iquique airport, 30 km from the station) and dv/v seasonal variations. Temperature data were first smoothed with a Savitzky–Golay filter of 30 days[34]. To approximate a periodical variation, we calculated the average temperature and velocity cycle by stacking the yearly temperature and dv/v time-series and fitting the average stack with a sinusoidal function (Figure S1). The fitting of the velocity data yields a first empirical correction of the thermal-induced velocity changes (red line in Fig. S3). The phase lag between the temperature and the velocity is equal to $\sim$ 19 days.

We assumed that the velocity changes originate from the thermal strain observed at one depth z due to thermal diffusion in a subsurface layer of thermal diffusivity κ. For a periodic temperature oscillation at the surface (of period ω), the phase lag for the temperature T at depth z can be retrieved with the following equation[35]:

$$T = T_0 + \Delta T \exp\left(-z\sqrt{\frac{\omega}{2\kappa}}\right) \cos\left(\omega t - z\sqrt{\frac{\omega}{2\kappa}}\right). \tag{1}$$

In this relation, one can see that the phase lag is equal to $-z\sqrt{\frac{\omega}{2\kappa}}$. From the phase difference calculated before and after setting the period ω to one year, we obtain the value of the ratio $z^2/2\kappa$, which determines the system. Assuming now a generic thermal diffusivity of $\kappa = 1.10^{-2}$ cm^2/s, we can model the velocity changes from the temperature observed at the characteristic depth of the ratio ($z = 1.25$ m). Plugging these values in a 1D thermal diffusion numerical simulation (computed with a forward Euler scheme) and using the surface temperature time-series (Fig. S2a), we obtained the temperature depth profiles shown in Figure S2b. We extracted the temperature at depth $z = 1.25$ m and scale it to the velocity changes through a factor α, which represent the expansion coefficient of the rocks in the subsurface. This scaling is done on the velocity data of 2007 prior to the Tocopilla earthquake. The velocity time-series from this simulation is shown in Figure S3a.

The retained temperature model for the paper is taken as the average between the two modeled dv/v time-series (Fig. S3a). Indeed, we combine the best of both corrections as **1.** the numerical correction is based on the temperature time-series and may have the best correction for the phase of the temperature-induced velocity changes and **2.** the amplitudes of the velocity changes is more consistent with the sinusoidal correction.

Measurement of τ_{max}: We used the expression of Snieder et al., 2016 to find the maximum relaxation timescale τ_{max}, which controls the duration of the recovery phase after earthquakes:

$$R(t) = \int_{\tau_{min}}^{\tau_{max}} \frac{1}{\tau} e^{-(t-t_0)/\tau} \, d\tau. \tag{2}$$

From equation (2), one can see that function $R(t)$ is therefore a superposition of exponential recoveries characterised by timescales τ. From a previous publication at the Patache field site[19], we know that the minimum relaxation timescale τ_{min} is inferior to one minute. At the daily time resolution of the retrieved velocity time-series of this study, we also do not resolve τ_{min}. Therefore, we fixed τ_{min} to one day and scaled $R(t)$ to the velocity measurements and find the best fitting τ_{max}.

We first quantified the relaxation time of the Iquique and Tocopilla earthquakes, assuming from Figure 1d that both earthquakes are followed by the same recovery timescale. Therefore, we averaged the first 1000 days of relaxation of both time-series (Fig. S4a) and interpolated the resulting recovery on a logarithmic x-axis. The latter step gives an equal weight to the early relaxation times in the fitting process. Finally, we fit and scaled the expression $R(t)$ and obtain a best fitting value of τ_{max} = 3887 d.

For each aftershock-induced recovery, τ_{max} was obtained by fitting the first 10 days of relaxation (Fig. S4b) without the interpolation step. We also report the τ_{max} values corresponding to $\pm$ 10% of the variance of the best fitting value (orange and green lines in Figure 2b).

Estimating the performance of the synthetic seismic velocity time-series For comparing the efficiency of the two models, we used the Nash-Sutcliffe efficiency (NSE) coefficient. The coefficient estimates the performance of a model at predicting a time-series relative to the mean of the time-series. This is calculated as

$$\text{NSE} = 1 - \frac{\sum(v - v_m)^2}{\sum(v - \bar{v})^2}. \tag{3}$$

In this equation, v is the time-series that we want to predict, v_m is the predicted time-series from a model and $\bar{v}$ is the mean of the observed time-series. We obtained NSE $= 0.68$ for the model featuring the exponential scaling and NSE $= -2.61$ for the model featuring the constant timescale of relaxation. The negative coefficient indicates that the model with the constant timescale of relaxation is less efficient at predicting the data than the mean of the seismic velocity changes.

State variable theory: We look for an equation that is homogeneous to the velocity changes and choose a form that is mathematically viable with the logarithmic evolution of the recovery. A general equation for the velocity variations dv/dt can be expressed as

$$\frac{dv}{dt}(t) = A \exp\left[-Bv(t)\right] - C, \tag{4}$$

where A, B and C are constants with A and C having the same dimension than dv/dt, and B having the dimension of $1/v$. Note that the expression (4) has the same form than Arrhenius equation[23], used to model thermal-induced processes and creep rates. The constant A is generally interpreted as the number of molecular collisions characteristic to the physical system at play while B is linked to the activation energy of the reaction. We have added C to impose a limit on the recovery at which the rate of velocity changes does not change anymore ($dv/dt = 0$) so that the recovery is complete. Based on the dimension of the constants, we further parametrise (4) to highlight a timescale τ: letting $B = 1/v^*$, $C = v^*/\tau$ and $A = v^* e^{v_\infty/v^*}/\tau$, we get

$$\frac{dv_\tau}{dt}(t) = \frac{v^*}{\tau}\left(\exp\left[-\frac{v_\tau(t) - v_\infty}{v^*}\right] - 1\right), \tag{5}$$

in which v_∞ is the steady state velocity value in the absence of earthquakes, v^* is a velocity modulating the prefactor and the exponential term and v_τ is the velocity associated with a certain relaxation time τ. We consider several contacts or flaws with different characteristic timescales τ, which affect the velocity changes. The total observed velocity change $v(t)$ is a function of these voids. The contribution of each v_τ to the total observed velocity changes $v(t)$ depends on the density of the associated voids/contacts and their respective sizes. For the sake of simplicity, we take in this paper the average of all v_τ dynamics present in the system:

$$v(t) = \frac{1}{N}\sum_{i=1}^{N} v_{\tau_i}(t) \tag{6}$$

To show the logarithmic evolution of our framework, we now derive the expression of the solution of (5) for initial condition $v_0 = v_\tau(0) < v_\infty$, and denote by $\Delta = v_\infty - v_0$ the size of the initial velocity drop. Letting $w(t) = \exp(-(v_\tau(t) - v_\infty)/v^*)$, there holds

$$\frac{dw}{dt}(t) = -\frac{1}{v^*}\frac{dv_\tau}{dt}(t) \times w(t) = -\frac{1}{\tau}(w(t) - 1) \times w(t) \tag{7}$$

which in turn yields

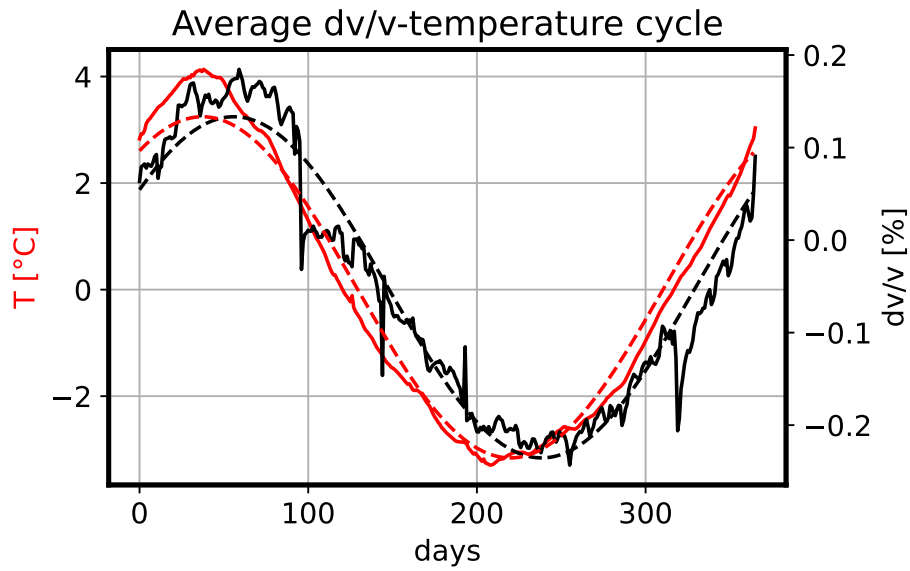$$\int_0^t \frac{dw}{w(w-1)} = -\int_0^t \frac{dt}{\tau} = -\frac{t}{\tau}. \tag{8}$$

The LHS of the above display can be expressed as

$$\int_0^t \frac{dw}{w(w-1)} = \int_0^t \left(\frac{1}{w-1} - \frac{1}{w}\right) dw = \left[\log\left(\frac{w-1}{w}\right)\right]_0^t = \log\left(\frac{w(0)(w(t)-1)}{(w(0)-1)w(t)}\right) \tag{9}$$

Letting $\xi_0 = (w(0) - 1)/w(0)$, we finally find that $w(t) - 1 = \xi_0 e^{-t/\tau} w(t)$, which immediately gives $w(t) = (1 - \xi_0 e^{-t/\tau})^{-1}$. Expressing w back as a function of v_τ finally yields

$$v_\tau(t) = v_\infty - v^* \log\left(1 - (1 - e^{-\Delta/v^*})e^{-t/\tau}\right). \tag{10}$$

Figure S1. *Average annual cycle of surface temperature and dv/v variations in Patache, Chile.* The red solid curve shows the average relative temperature variation of the surface temperature time-series (shown in figure S2a). The solid black line shows the annual average for the *dv/v* variations. Dashed lines correspond to the sinusoidal fits of the data. The phase lag between the temperature and the seismic velocity response is equal to ~ 19 days.
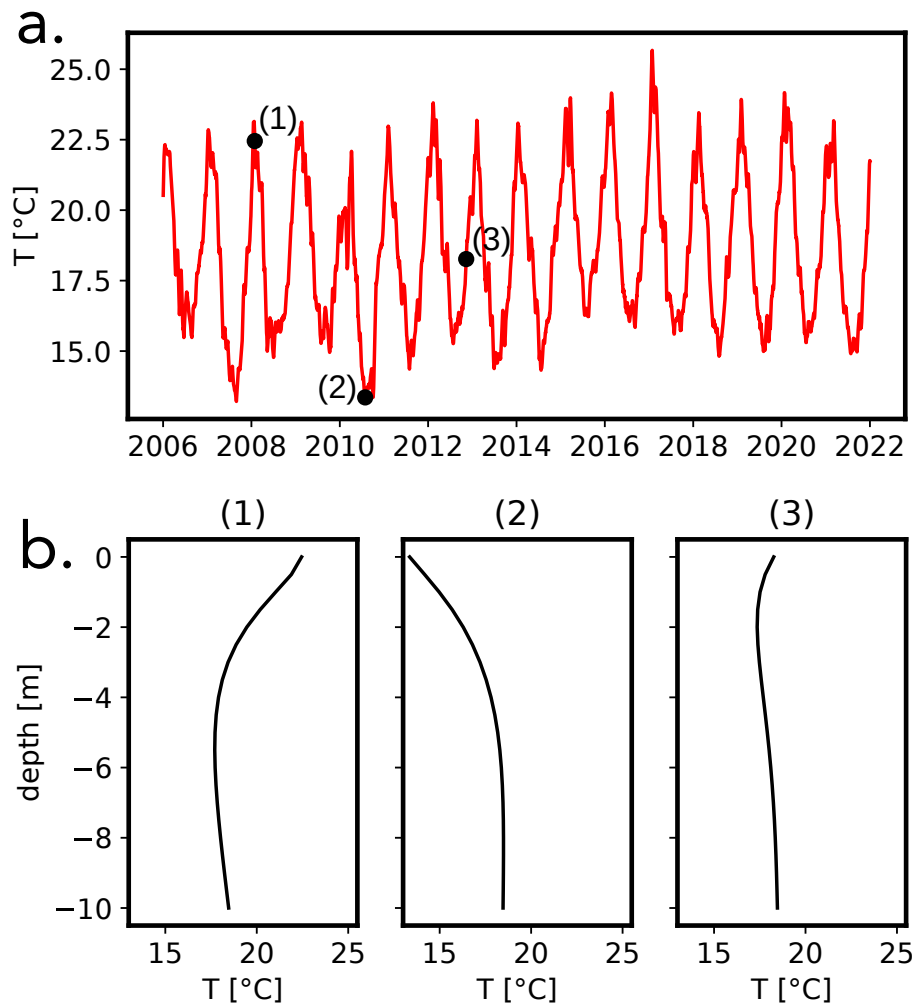
Figure S2. *Numerical simulation of the temperature diffusion under the seismic site.* **a.** shows the temperature time-series used in this study (taken at Iquique airport, ~ 30 km from the PATCX station) to construct the dv/v models. The numbers indicate different dates for which the modelled temperature depth-profiles are shown in **b**.
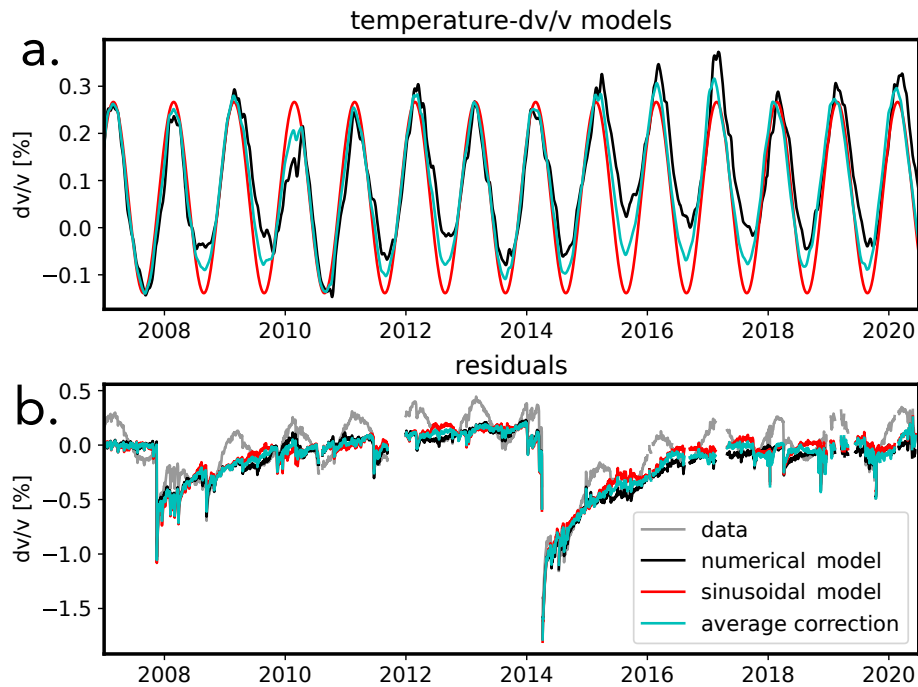
Figure S3. *Temperature-induced dv/v models* **a.** The solid lines show the different models for correcting the velocity changes due to surface temperature variations. The legend for the colours is indicated on the lower plot. **b.** The coloured lines represent the residuals of the data after correction for temperature effect sby the models shown on plot **a**. The raw data is shown in grey.
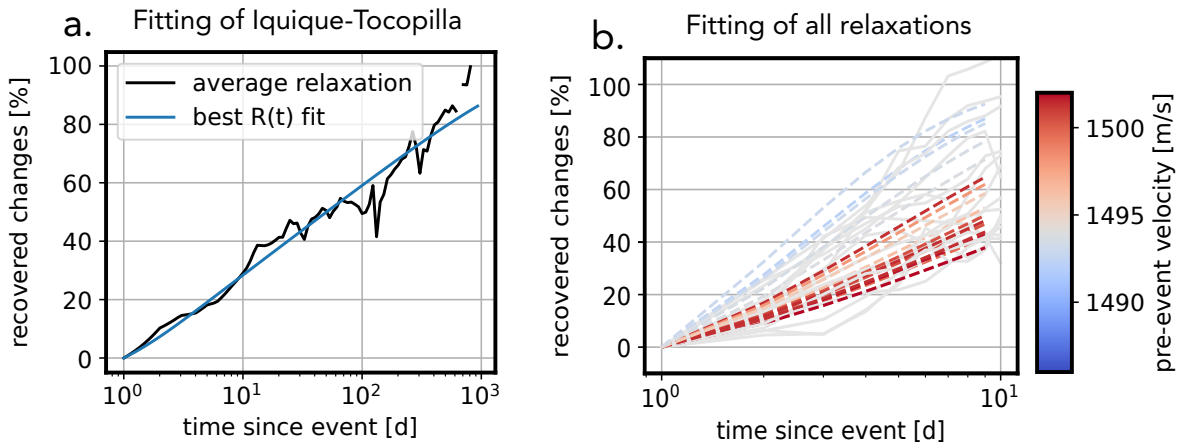
Figure S4. *Fitting of recoveries with the relaxation function R(t)* **a.** The black line shows the interpolated average velocity recovery observed after Tocopilla and Iquique earthquakes. The blue line shows the best $R(t)$ fit with $\tau_{max} = 3887$ d. **b.** Fitting of all aftershocks-induced recoveries. The dashed lines indicate the fits. The pre-event velocity before the earthquakes are indicated in colours.
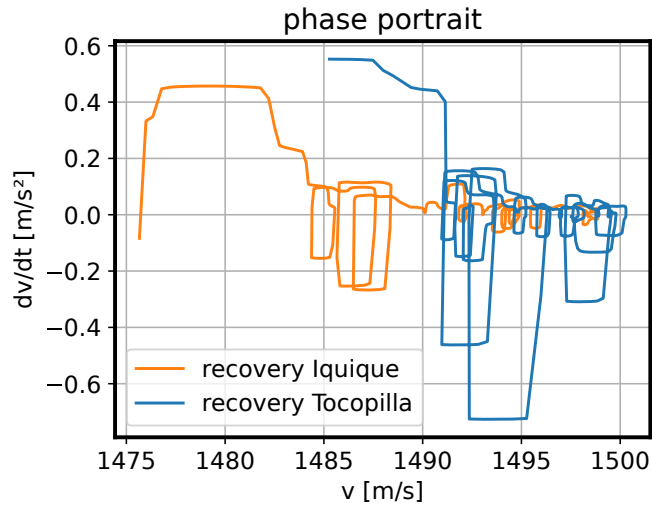
Figure S5. *Phase portrait of the velocity changes observed after the Tocopilla and Iquique earthquakes.* Both lines were computed for the recoveries shown in Figure 1c. The derivative dv/dt was obtained using the total-variation regularisation method[36].

Table S1. Aftershocks Information

date	mw	lat	lon
16.12.2007	6.7	-22.89	-70.13
04.02.2008	6.3	-20.19	-69.95
16.02.2008	6.1	-21.32	-68.36
01.03.2008	5.6	-20.31	-69.98
24.03.2008	6.2	-20.08	-68.97
10.09.2008	5.7	-20.3	-69.18
17.04.2009	6.1	-19.58	-70.5
15.07.2009	5.3	-20.38	-69.15
13.11.2009	6.9	-19.41	-70.3
22.10.2010	5.7	-20.83	-68.45
20.06.2011	6.5	-21.64	-68.35
10.03.2012	5.2	-19.67	-69.15
07.01.2014	5.3	-21.03	-69.61
23.03.2014	6.2	-19.7	-70.78
30.05.2014	5.6	-21.29	-70
13.07.2014	5.6	-20.26	-70.35
14.08.2014	5.3	-19.86	-69.86
10.10.2017	6.3	-18.52	-69.64
05.04.2018	5.6	-20.38	-70.61